Al-nahari, Azzam; Jäntti, Riku; Mishra, Deepak; Hämäläinen, Jyri

# Massive MIMO Beamforming in Monostatic Backscatter Multi-Tag Networks

*Published in:*
IEEE Communications Letters

*DOI:*
10.1109/LCOMM.2020.3046690

Published: 01/04/2021

*Document Version*
Publisher's PDF, also known as Version of record

# Massive MIMO Beamforming in Monostatic Backscatter Multi-Tag Networks

Azzam Al-Nahari, Riku Jäntti, *Senior Member, IEEE*, Deepak Mishra, *Member, IEEE*, and Jyri Hämäläinen, *Senior Member, IEEE*

***Abstract*— This letter investigates the role of massive multiple-input multiple-output (MIMO) in improving the spectral and energy efficiency of monostatic backscatter communication systems, where a multiple-antenna reader aims to decode information backscattered from multiple tags. Specifically, we investigate the performance of the two most prominent precoders and combiners, namely, the matched filter and zero forcing. First, we derive capacity lower bounds for the four different underlying transceiver design configurations. Then, asymptotic analysis is conducted and it is shown that with perfect channel state information, the total transmit power can be scaled down by a factor of the square of the number of transmit antennas without loss in the performance. To further corroborate the practical utility of the considered massive MIMO multi-tag setting, the optimization of the backscatter coefficients for sum rate maximization and the effect of imperfect channel state information are also considered.**

***Index Terms*— Monostatic backscatter communications, massive MIMO, beamforming, sum rate.**

## I. Introduction

With the emergence of Internet-of-Things (IoT) networks, one of the key challenges is the limited service lifetime of the IoT devices. Backscatter communications have been considered a promising technology that can help in sustaining the IoT devices and enhancing network lifetime [1]. There are mainly three types of backscatter communications: monostatic, bi-static, and ambient backscattering [2]. The major bottlenecks for these techniques are the limited communication range and low achievable rates [3]. The work in [4] investigated a numerical approach to maximize the sum-backscattered rate to multi-antenna reader by jointly optimizing the transceiver design at the reader and the backscattering coefficients at the tags, assuming perfect channel state information (CSI) at the reader. Channel estimation of monostatic backscattering setup for single tag was studied in [5].

Massive multiple-input multiple-output (MIMO) is considered a key technology for next generation wireless networks with various scenarios [6]. The *spatial multiplexing gain* of massive MIMO is crucial to spatially multiplex a large number of distributed devices and *energy efficiency* is important for power-limited devices [7]. The work in [8] studied energy beamforming in massive MIMO backscatter communication systems. However, the objective of the mentioned work is the wireless power transfer (WPT) by leveraging the retrodirectivity of the large antenna elements and backscattering at the energy receivers. The potential of massive MIMO in improving the spectral and energy efficiency of backscatter communications has not been investigated yet in the literature.

In this letter, we will have a first look at the role of massive MIMO in monostatic multi-tag backscatter communications. The performance of matched filter (MF) and zero forcing (ZF) precoders and combiners in terms of the sum rate is studied. The contribution of this work is summarized as follows.

1) This letter is one of the early attempts to investigate the performance gain of massive MIMO beamforming in multi-tag backscatter communication systems. We investigate four different transceiver design configurations using MF and ZF beamforming techniques.
2) We derive tight closed-form capacity lower bounds on the achievable backscattered sum rate for the different beamforming schemes to highlight the effect of the different system parameters on the performance.
3) We present asymptotic analysis for these derived capacity expressions to shed novel key insights on massive MIMO based improvements in terms of spectral and energy efficiency of the multi-tag backscattering systems. In particular, we show that when the number of transmit antennas, as denoted by $M$, grows without bound, by using perfect CSI at the reader, we can scale down its transmit power by a factor of $M^2$.
4) To maximize backscattered rate, we derive the optimal backscattering coefficients at the tags for the different schemes and verify the proposed analytical claims via extensive simulations.

## II. System and Channel Models

We consider a monostatic backscatter communication system as shown in Fig. 1, which consists of a reader $\mathcal{R}$ equipped with $M$ antennas and $K$ single-antenna tags. The $k$-th tag is denoted by $\mathcal{T}_k$, with $k \in \Phi \triangleq \{1, 2, \ldots, K\}$. The tags are assumed to be uniformly distributed over a square of length $2R$ and $\mathcal{R}$ is placed in the center. The channel fading matrix from $\mathcal{R}$ to the $K$ tags is denoted as $\mathbf{H} \in \mathbb{C}^{M \times K}$, where the $k$-th column vector $\mathbf{h}_k \sim \mathcal{CN}(\mathbf{0}_{M\times 1}, \beta_k \mathbf{I}_M)$ represents the channel fading from $\mathcal{R}$ to $\mathcal{T}_k$. The parameter $\beta_k$ represents the large-scale path loss of $\mathcal{T}_k - \mathcal{R}$ link. In this letter, we have assumed that the CSI is available at $\mathcal{R}$. In case of passive or semi-passive tags, channel estimation can be done at $\mathcal{R}$ using backscattering during the training phase [5].

Manuscript received November 17, 2020; accepted December 11, 2020. Date of publication December 22, 2020; date of current version April 9, 2021. This work has been partly funded by the Academy of Finland project ABACUS (#319003). The associate editor coordinating the review of this letter and approving it for publication was H. Zhang. *(Corresponding author: Azzam Al-Nahari.)*

Azzam Al-Nahari is with the Department of Communications and Networking, Aalto University, 02150 Espoo, Finland, and also with the Department of Electrical Engineering, Ibb University, Ibb, Yemen (e-mail: azzamyn@gmail.com).

Riku Jäntti and Jyri Hämäläinen are with the Department of Communications and Networking, Aalto University, 02150 Espoo, Finland (e-mail: riku.jantti@aalto.fi; jyri.hamalainen@aalto.fi).

Deepak Mishra is with the School of Electrical Engineering and Telecommunications, University of New South Wales (UNSW), Sydney, NSW 2052, Australia (e-mail: d.mishra@unsw.edu.au).

Digital Object Identifier 10.1109/LCOMM.2020.3046690

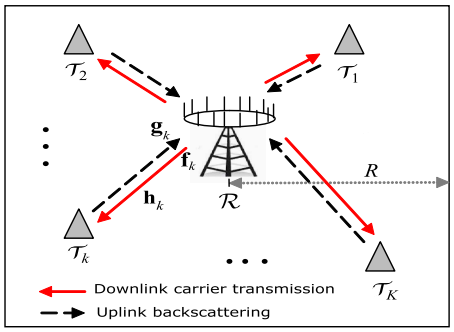


Fig. 1. Illustration of a massive MIMO monostatic backscatter communication system.

The effect of imperfect CSI on the performance is discussed in Section IV-C. In the following, the superscripts $*$, T, and H denote the conjugate, transpose, and conjugate transpose, respectively.

The reader transmits a single carrier signal $s$ to power up the $K$ tags concurrently, where $\mathbb{E}[|s|^2]=1$, by assigning each tag $\mathcal{T}_k$ a precoding vector $\mathbf{f}_k \in \mathbb{C}^{M\times 1}$, $k\in\Phi$. The reflected data symbols from the tags are then spatially separated at $\mathcal{R}$ with the aid of $K$ linear decoding vectors $\mathbf{g}_i \in \mathbb{C}^{M\times 1}$, $i\in\Phi$, where $\mathbf{g}_k$ is used for decoding $\mathcal{T}_k$'s message. Moreover, the receiver at $\mathcal{R}$ is assumed to operate in full duplex mode.[1] The received baseband signal at $\mathcal{T}_k$ is expressed as

$$y_{\mathcal{T}_k} = \sqrt{\mathrm{P}}\mathbf{h}_k^{\mathrm{T}}\mathbf{x} + n_{\mathcal{T}_k}, \tag{1}$$

where $P$ is the total transmit power budget at $\mathcal{R}$ and $n_{\mathcal{T}_k} \sim \mathcal{CN}(0,\sigma_{\mathcal{T}}^2)$ is the additive white Gaussian noise (AWGN) at $\mathcal{T}_k$. $\mathbf{x}=\frac{1}{\sqrt{\psi}}\sum_{i=1}^{K}\mathbf{f}_i s$ is the $M\times 1$ transmitted vector, obtained by applying the precoding vectors $\mathbf{f}_i$, $\forall i\in\Phi$ to the carrier signal $s$, and $\psi$ is a long-term normalization factor that ensures $\mathbb{E}[\|\mathbf{x}\|^2]=1$. Equivalently, we can write

$$\psi = \mathbb{E}\Big[\big\|\sum\nolimits_{i\in\Phi}\mathbf{f}_i\big\|^2\Big] = \mathbb{E}\Big[\mathrm{Tr}\left(\mathbf{F}^{\mathrm{H}}\mathbf{F}\right)\Big], \tag{2}$$

where $\mathbf{F}\triangleq[\mathbf{f}_1\,\mathbf{f}_2\,\ldots\,\mathbf{f}_K]\in\mathbb{C}^{M\times K}$.

Let $b_k$ be the effective information signal of $\mathcal{T}_k$ $\forall k\in\Phi$, with $\mathbb{E}[|b_k|^2]=\alpha_k$, where $\alpha_k$ is the reflection coefficient of $\mathcal{T}_k$.[2] Noting that the backscattered noise $n_{\mathcal{T}_k}$ is practically negligible compared to the power of the reflected carrier [3], [8], the received signal at $\mathcal{R}$ is then given by

$$\begin{aligned}\mathbf{y}_{\mathcal{R}} &= \sum\nolimits_{j\in\Phi}\mathbf{h}_j y_{\mathcal{T}_j} b_j + \mathbf{n}_{\mathcal{R}}\\ &\approx \sqrt{\tfrac{P}{\psi}}\sum\nolimits_{j\in\Phi}\mathbf{h}_j\mathbf{h}_j^{\mathrm{T}} b_j \sum\nolimits_{i\in\Phi}\mathbf{f}_i s_i + \mathbf{n}_{\mathcal{R}},\end{aligned} \tag{3}$$

where $\mathbf{n}_{\mathcal{R}}\sim\mathcal{CN}(\mathbf{0}_{M\times 1},\sigma_{\mathcal{R}}^2\mathbf{I}_M)$ is the AWGN at $\mathcal{R}$. After applying the linear detection matrix $\mathbf{G}=[\mathbf{g}_1\,\mathbf{g}_2\,\ldots\,\mathbf{g}_K]\in\mathbb{C}^{M\times K}$, we get

$$\hat{\mathbf{y}}_{\mathcal{R}} = \mathbf{G}^{\mathrm{H}}\mathbf{y}_{\mathcal{R}}. \tag{4}$$

[1]Note that as the reader $\mathcal{R}$ transmits unmodulated single carrier signal, the receiver can easily decouple its own self-jamming carrier, which is a commonplace in the literature [5], [9], [10], [11, Sec. V], and is considered in our work in this letter.

[2]The standard Shannon capacity formula used in this letter assumes that the tag uses a Gaussian codebook with constrained mean reflected power $\alpha_k$ [4], which is assumed to incorporate a reflection amplifier as studied in [12].

From the $k$-th element of $\hat{\mathbf{y}}_{\mathcal{R}}$, the received signal-to-interference-and-noise ratio (SINR) of $\mathcal{T}_k$ can be obtained as

$$\gamma_{\mathcal{R}_k}^{\mathrm{a,b}} = \frac{\alpha_k\left|\mathbf{g}_k^{\mathrm{H}}\mathbf{h}_k\right|^2\sum_{i\in\Phi}\left|\mathbf{h}_k^{\mathrm{T}}\mathbf{f}_i\right|^2}{\sum_{j\in\Phi_k}\alpha_j\left|\mathbf{g}_k^{\mathrm{H}}\mathbf{h}_j\right|^2\sum_{i\in\Phi}\left|\mathbf{h}_j^{\mathrm{T}}\mathbf{f}_i\right|^2+\frac{\psi\sigma_{\mathcal{R}}^2}{P}\left\|\mathbf{g}_k\right\|^2}, \tag{5}$$

where $\mathrm{a,b}\in\{\mathrm{MF},\mathrm{ZF}\}$ denotes the precoder/combiner and $\Phi_k\triangleq\Phi\backslash\{k\}=\{1,2,\ldots,k-1,k+1,k+2,\ldots K\}$. The average rate of $\mathcal{T}_k$ is given as

$$R_k^{\mathrm{a,b}} = \mathbb{E}\big[\log_2\big(1+\gamma_{\mathcal{R}_k}^{\mathrm{a,b}}\big)\big]. \tag{6}$$

Using Jensen's inequality, a lower bound on $R_k^{\mathrm{a,b}}$ is given by

$$R_k^{\mathrm{a,b}} \geq \underline{R}_k^{\mathrm{a,b}} = \log_2\Big(1+\big(\mathbb{E}[1/\gamma_{\mathcal{R}_k}^{\mathrm{a,b}}]\big)^{-1}\Big). \tag{7}$$

Finally, the the resulting backscattered sum rate is given as

$$R_{\mathrm{sum}}^{\mathrm{a,b}} = \sum\nolimits_{k\in\Phi} R_k^{\mathrm{a,b}}. \tag{8}$$

## III. Capacity Lower Bounds for Matched Filter and Zero Forcing Precoders and Combiners

In this section, we derive capacity lower bounds for MF and ZF precoders and combiners, which are given below in (9) and (10), respectively

$$\mathbf{F} = \begin{cases}\mathbf{H}^* & \text{for MF} \quad (9a)\\ \mathbf{H}^*\left(\mathbf{H}^{\mathrm{T}}\mathbf{H}^*\right)^{-1} & \text{for ZF} \quad (9b)\end{cases}$$

$$\mathbf{G} = \begin{cases}\mathbf{H} & \text{for MF} \quad (10a)\\ \mathbf{H}\left(\mathbf{H}^{\mathrm{H}}\mathbf{H}\right)^{-1} & \text{for ZF} \quad (10b)\end{cases}$$

### A. MF Precoder and MF Combiner (MF-MF)

In this case, from (2) and (9a), we get $\psi = M\sum_{i\in\Phi}\beta_i$. Using (9a) and (10a) in (5), and using asymptotic massive MIMO expressions [8], [13], i.e., $\frac{1}{M}\left\|\mathbf{h}_j\right\|^4\to(M+1)\beta_j^2$ and $\frac{1}{M}\left|\mathbf{h}_j^{\mathrm{T}}\mathbf{h}_i^*\right|^2\to\beta_j\beta_i$ ( $\forall i\neq j$), it can be shown that

$$\gamma_{\mathcal{R}_k}^{\mathrm{MF,MF}} = \frac{\alpha_k\theta_k\left\|\mathbf{h}_k\right\|^2}{\sum_{j\in\Phi_k}\alpha_j\theta_j\left|\frac{\mathbf{h}_k^{\mathrm{H}}}{\|\mathbf{h}_k\|}\mathbf{h}_j\right|^2+\frac{\sigma_{\mathcal{R}}^2}{P}\sum_{i\in\Phi}\beta_i}, \tag{11}$$

where $\theta_m=(M+1)\beta_m^2+\beta_m\sum_{i\in\Phi_m}\beta_i$. From (7) and (11), and following similar steps as those for proving Proposition 2 in [7], a lower bound on $R_k^{\mathrm{MF,MF}}$ is derived as

$$\underline{R}_k^{\mathrm{MF,MF}} = \log_2\left(1+\frac{\alpha_k\beta_k\theta_k(M-1)}{\sum_{j\in\Phi_k}^{K}\alpha_j\beta_j\theta_j+\frac{\sigma_{\mathcal{R}}^2}{P}\sum_{i\in\Phi}\beta_i}\right). \tag{12}$$

### B. MF Precoder and ZF Combiner (MF-ZF)

With ZF combiner, $\mathbf{G}^{\mathrm{H}}\mathbf{H}=\mathbf{I}_K$. Thus, $\mathbf{g}_k^{\mathrm{H}}\mathbf{h}_i=1$ when $i=k$, and zero otherwise. Substituting these results in (5) and using the asymptotic expressions before (11), we get

$$\gamma_{\mathcal{R}_k}^{\mathrm{MF,ZF}} = \frac{\alpha_k\theta_k P}{\sigma_{\mathcal{R}}^2\sum_{i=1}^{K}\beta_i.\left\|\mathbf{g}_k\right\|^2}. \tag{13}$$

Using (7), a lower bound on $R_k^{\mathrm{MF,ZF}}$ can be obtained as

$$\underline{R}_k^{\mathrm{MF,ZF}} = \log_2\left(1+\frac{\alpha_k\theta_k P}{\sigma_{\mathcal{R}}^2\sum_{i\in\Phi}\beta_i\mathbb{E}\big[(\mathbf{H}^{\mathrm{H}}\mathbf{H})^{-1}\big]_{kk}}\right) = \log_2\left(1+\frac{\alpha_k\beta_k\theta_k(M-K)P}{\sigma_{\mathcal{R}}^2\sum_{i\in\Phi}\beta_i}\right), \quad (14)$$

where the last equality is obtained since $\mathbb{E}\big[(\mathbf{H}^{\mathrm{H}}\mathbf{H})^{-1}\big]_{kk} = \frac{1}{\beta_k}\mathbb{E}\big[(\mathbf{Z}^{\mathrm{H}}\mathbf{Z})^{-1}\big]_{kk} = \frac{1}{K\beta_k}\mathbb{E}\big[(\mathbf{Z}^{\mathrm{H}}\mathbf{Z})^{-1}\big] \overset{(a)}{=} \frac{1}{(M-K)\beta_k}$, where $\mathbf{Z}$ has i.i.d $\mathcal{CN}(0,1)$ entries. Equality $(a)$ is obtained because $\mathbf{Z}^{\mathrm{H}}\mathbf{Z}$ is a central complex Wishart matrix [14, Lemma 2.10].

### C. ZF Precoder and ZF Combiner (ZF-ZF)

In this case, $\psi = \mathbb{E}\big[\mathrm{Tr}\left(\mathbf{H}^{\mathrm{T}}\mathbf{H}^{*}\right)^{-1}\big]$. From [14], we see $\psi = \frac{\sum_{i\in\Phi}\frac{1}{\beta_i}}{(M-K)}$. Substituting (9b) and (10b) in (5), we get

$$\gamma_{\mathcal{R}_k}^{\mathrm{ZF,ZF}} = \frac{\alpha_k(M-K)P}{\sigma_{\mathcal{R}}^2\sum_{i\in\Phi}\frac{1}{\beta_i}.\left\|\mathbf{g}_k\right\|^2}. \quad (15)$$

As in (14), a lower bound on $R_k^{\mathrm{ZF,ZF}}$ is obtained as

$$\underline{R}_k^{\mathrm{ZF,ZF}} = \log_2\Big(1+\frac{\alpha_k\beta_k(M-K)^2P}{\sigma_{\mathcal{R}}^2\sum_{i\in\Phi}\frac{1}{\beta_i}}\Big). \quad (16)$$

### D. ZF Precoder and MF Combiner (ZF-MF)

The SINR of the ZF-MF scheme can be written as

$$\gamma_{\mathcal{R}_k}^{\mathrm{ZF,MF}} = \frac{\alpha_k\left\|\mathbf{h}_k\right\|^2}{\sum_{j\in\Phi_k}\alpha_j\big|\frac{\mathbf{h}_k^{\mathrm{H}}}{\|\mathbf{h}_k\|}\mathbf{h}_j\big|^2+\frac{\sigma_{\mathcal{R}}^2\sum_{i\in\Phi}\frac{1}{\beta_i}}{(M-K)P}}. \quad (17)$$

Following similar steps as those for obtaining (12), we get

$$\underline{R}_k^{\mathrm{ZF,MF}} = \log_2\left(1+\frac{\alpha_k\beta_k(M-1)}{\sum_{j\in\Phi_k}\alpha_j\beta_j+\frac{\sigma_{\mathcal{R}}^2}{P}\frac{\sum_{i\in\Phi}\frac{1}{\beta_i}}{(M-K)}}\right). \quad (18)$$

## IV. Asymptotic Analysis and Optimization

In this section, we provide implications of the derived results, and conduct asymptotic analysis when $M$ grows without bounds. This reveals massive MIMO capabilities in improving the spectral and energy efficiency of backscatter systems. The optimal backscatter coefficients are also derived.

### A. Implications and Asymptotic Analysis

*1) Spectral Efficiency Comparison:* It can be noted from (14) and (16) that the achievable rates of MF-ZF and ZF-ZF schemes are proportional with $(M+1)(M-K)$ and $(M-K)^2$, respectively. This is not the case with MF-MF and ZF-MF, as seen from (12) and (18). Therefore, the performance is expected to be much better considering ZF combiner rather than MF as $M$ increases. On the other hand, with fixed $M$ and asymptotic low SNR values in (12) and (18), the interference terms in the denominator can be neglected compared to the AWGN. Therefore, MF-MF and ZF-MF schemes are expected to achieve comparable performance in this SNR regime.

*2) Asymptotic Power Efficiency:* Let us consider the case when $M\to\infty$, and assume that the total power $P$ is scaled such that $P \triangleq \frac{p}{M^2}$. Defining $\underline{R}_{k,\infty}^{\mathrm{a,b}} \triangleq \lim_{M\to\infty}\underline{R}_k^{\mathrm{a,b}}(p)$, we get

$$\underline{R}_{k,\infty}^{\mathrm{MF,MF}} = \underline{R}_{k,\infty}^{\mathrm{MF,ZF}} = \log_2\left(1+\frac{\alpha_k\beta_k^3 p}{\sigma_{\mathcal{R}}^2\sum_{i\in\Phi}\beta_i}\right), \quad (19)$$

$$\underline{R}_{k,\infty}^{\mathrm{ZF,ZF}} = \underline{R}_{k,\infty}^{\mathrm{ZF,MF}} = \log_2\left(1+\frac{\alpha_k\beta_k p}{\sigma_{\mathcal{R}}^2\sum_{i\in\Phi}\frac{1}{\beta_i}}\right). \quad (20)$$

To get more insight, and without loss of generality, consider that all tags has the same large scale fading $\beta$. Then, the rates in (19) and (20) will be $\underline{R}_{k,\infty}^{\mathrm{a,b}} = \log_2\Big(1+\frac{\alpha_k\beta^2 p}{\sigma_{\mathcal{R}}^2 K}\Big)$, $\forall \mathrm{a},\mathrm{b}\in\{\mathrm{MF},\mathrm{ZF}\}$. This last equation implies that with perfect CSI and $M\to\infty$, the performance of backscatter multi-tag massive MIMO system with total transmit power of $\frac{p}{M^2}$ at $\mathcal{R}$ is equal to the performance of single-input single-output (SISO) system with transmit power of $\frac{p}{K}$ for each tag, without any interference and without fast fading. In other words, by using large number of transmit antennas, we can scale down the transmit power at $\mathcal{R}$ by a factor $M^2$, and at the same time increase the spectral efficiency $K$ times by serving $K$ tags in the same time-frequency resource.

### B. Optimization of Backscattering Coefficients at the Tags

For a given number of tags $K$, and defining $\boldsymbol{\alpha} = [\alpha_1\ \alpha_2\ \ldots\ \alpha_K]^{\mathrm{T}}$, the optimization problem that maximizes the sum rate for the reflection coefficients can be written as

$$\mathcal{O}_1: \underset{\boldsymbol{\alpha}}{\text{maximize}}\ R_{\mathrm{sum}}^{\mathrm{a,b}};\ \ \mathrm{s.t.}: \alpha_{\min}\le\alpha_{\mathrm{k}}\le\alpha_{\max},\quad \forall k\in\Phi,$$

where $\alpha_{\min}\ge 0$ and $\alpha_{\max}\le 1$ [15]. It is clear from (8), (14), and (16) that $R_{\mathrm{sum}}^{\mathrm{MF,ZF}}$ and $R_{\mathrm{sum}}^{\mathrm{ZF,ZF}}$ are monotonically increasing in each $\alpha_k$, $\forall k\in\Phi$. Therefore, the optimal backscatter coefficients for ZF-MF and ZF-ZF are $\alpha_k^\star = \alpha_{\max}, \forall k\in\Phi$.

However, $\mathcal{O}_1$ is not convex for MF-MF and ZF-MF. Therefore, we will consider asymptotic optimization for both low and high SNR. The underlying results are given in Lemma 1.

*Lemma 1: For MF-MF and ZF-MF, under low-SNR regime, the optimal backscatter coefficient for each tag $\mathcal{T}_k$ is $\alpha_k^\star = \alpha_{\max}$, and under high-SNR, $\alpha_k^\star$ is characterized by binary power allocation, i.e., either $\alpha_k^\star = \alpha_{\max}$ or $\alpha_k^\star = \alpha_{\min}$.*

*Proof:* For low SNR setting, as the backscattered signals from the interfering tags is relatively very low in comparison to the received AWGN, we can use the approximations $\sum_{j\in\Phi_k}^{K}\alpha_j\beta_j\theta_j+\frac{\sigma_{\mathcal{R}}^2}{P}\sum_{i\in\Phi}\beta_i\approx\frac{\sigma_{\mathcal{R}}^2}{P}\sum_{i\in\Phi}\beta_i$ and $\sum_{j\in\Phi_k}\alpha_j\beta_j+\frac{\sigma_{\mathcal{R}}^2}{(M-K)P}\sum_{i\in\Phi}\frac{1}{\beta_i}\approx\frac{\sigma_{\mathcal{R}}^2}{(M-K)P}\sum_{i\in\Phi}\frac{1}{\beta_i}$ in (12) and (18), respectively. As a result, the corresponding bounds are monotonically increasing in each $\alpha_k$, or $\alpha_k^\star = \alpha_{\max}, \forall k\in\Phi$. For high SNR setting, it can be inferred from (12) and (18) that the rates saturate as $\frac{P}{\sigma_{\mathcal{R}}^2}\to\infty$. Therefore, for $\mathrm{a}\in\{\mathrm{MF},\mathrm{ZF}\}$ and $\mathrm{b}=\mathrm{MF}$, and over the range of high $\frac{P}{\sigma_{\mathcal{R}}^2}$ values, we can use the approximation $\log_2(1+\gamma_{\mathcal{R}_k}^{\mathrm{a,b}})\approx\xi_k\gamma_{\mathcal{R}_k}^{\mathrm{a,b}}$, where $\xi_k$ is constant. Thus, $R_{\mathrm{sum}}^{\mathrm{a,b}}\approx\sum_{k\in\Phi}\xi_k\gamma_{\mathcal{R}_k}^{\mathrm{a,b}}$. Now, it can be easily shown that $\frac{\partial^2 R_{\mathrm{sum}}^{\mathrm{a,b}}}{\partial\alpha_k^2}>0$, and hence $R_{\mathrm{sum}}^{\mathrm{a,b}}$ is strictly convex in $\alpha_k$. As the maximum value of a convex function lies at the corner points of its underlying variable

defined under the box constraints, we conclude that $\alpha_k^\star$ takes the values either $\alpha_{\max}$ or $\alpha_{\min}$. □

### C. Effect of Imperfect Channel State Information Knowledge

In this letter, we considered that perfect CSI is available at $\mathcal{R}$ and focused on finding performance bounds and optimizing the reflection coefficients at tags. However, in practice, channel estimation techniques need to be designed to obtain CSI. This is particularly challenging in backscatter communication systems where passive and semi-passive tags cannot actively transmit pilot signals to the reader. In [5], channel estimation techniques were proposed for the monostatic backscatter communication system with multi-antenna reader and single-antenna tag. Using the tag switching based pilot-signal backscattering from the tags [16], where only one tag is active during a sub-phase of the channel estimation phase, we can obtain the estimate for each $\mathbf{h}_k$ as $\hat{\mathbf{h}}_k$.

Now, we consider the case that $\mathcal{R}$ has imperfect knowledge of $\mathbf{h}_k$ for each $\mathcal{T}_k$. Thus, $\hat{\mathbf{h}}_k$ can be modeled as [17]

$$\hat{\mathbf{h}}_k = \sqrt{1-\eta^2}\mathbf{h}_k + \eta\sqrt{\beta_k}\mathbf{z}_k, \quad \forall k \in \Phi \tag{21}$$

where $\mathbf{z}_k \sim \mathcal{CN}(\mathbf{0}_{M\times 1}, \mathbf{I}_M)$ accounts for channel estimation errors independent of $\mathbf{h}_k$, and $0 \leqslant \eta \leqslant 1$ is a CSI parameter that indicates the quality of the instantaneous CSI, i.e., $\eta = 0$ corresponds to perfect instantaneous CSI and $\eta = 1$ corresponds to having only statistical channel knowledge.

It should be noted that capacity lower bounds and asymptotic analysis for the imperfect CSI case can be derived following similar steps as those presented in Sections IV and V, respectively, and using the estimated channel vector $\hat{\mathbf{h}}_k$ for each $\mathcal{T}_k$ instead of $\mathbf{h}_k$. However, due to limited space, a detailed discussion will be considered as an extension of our proposals in this letter in future work. In the next section, the effect of imperfect CSI will be investigated via simulation study, as considered in [4], [17], [18].

## V. Numerical Results

In this section, we numerically evaluate the performance of the proposed schemes. Unless otherwise stated, we set $P = 30\text{dBm}$ and $\sigma^2 = -140\text{dBm}$. As in [4], we consider $\alpha_{\min} = 0.01$ and $\alpha_{\max} = 0.078$. $\beta_k = \varrho d_k^{-\vartheta}$, where $\varrho = (\frac{3\times 10^8}{4\pi f})^2$ is the average channel attenuation at unit reference distance with $f = 915\text{MHz}$ [5] being the transmit frequency, $d_k$ is the $\mathcal{R}$ to $\mathcal{T}_k$ distance, and $\vartheta = 3$ is the path loss exponent.

In Fig. 2, the sum rate is plotted versus $M$ for the different scenarios. It is seen that the performance when using ZF as a combiner outperforms that when using MF. This is because using ZF combiner can eliminate the inter-tag interference received at $\mathcal{R}$. Note that ZF-ZF outperforms MF-ZF at high values of $M$. Note also that the simulation results match well with the numerical results of the derived lower bounds.

Fig. 3 depicts the sum rate against different effective backscattered SNR $\gamma \triangleq \frac{P\bar{\beta}^2}{\sigma^2_{\mathcal{R}}}$ values, with $\bar{\beta}^2 \triangleq \frac{1}{K}\sum_{i\in\Phi}\beta_i^2$. As shown, for MF-MF and ZF-MF, the rate gradually increases with $\gamma$ before it saturates, whereas, for MF-ZF and ZF-ZF, it increases indefinitely with $\gamma$. The effect of optimizing the backscatter coefficients is also shown, where full reflection mode (i.e., $\alpha_k = \alpha_{\max}$) achieves the optimal

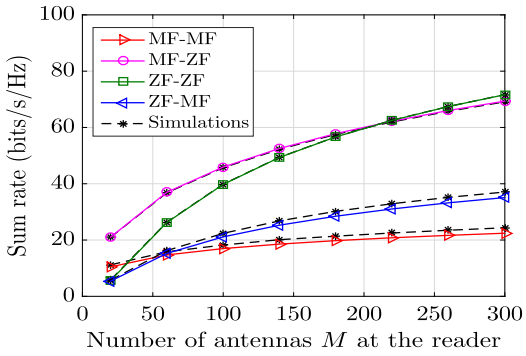


Fig. 2. Lower bounds and numerically evaluated values of the sum rate of the different schemes for different values of $M$; $K = 10$ and $R = 100$.

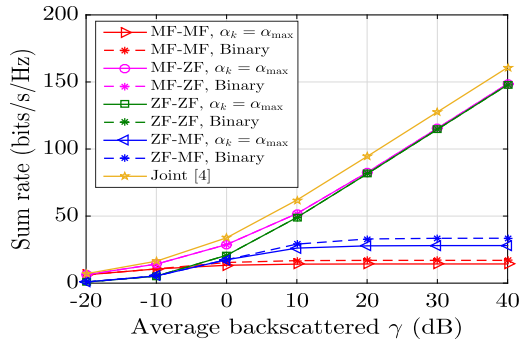


Fig. 3. Sum rate of the different schemes versus the backscattered SNR $\gamma \triangleq \frac{P\bar{\beta}^2}{\sigma^2}$ with $M = 100$, $K = 10$, and $R = 100$m.

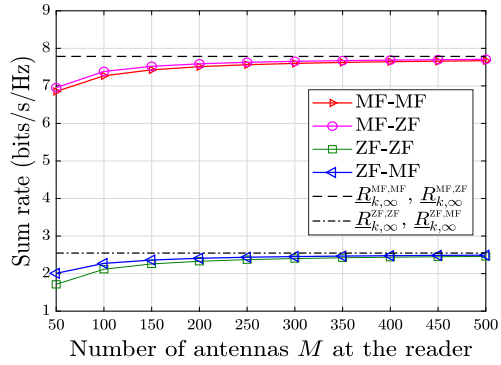


Fig. 4. Sum rate of the different schemes versus the number of antennas $M$, with $P \triangleq \frac{p}{M^2}$, $K = 10$, $R = 100$m, and $\frac{p\bar{\beta}^2}{\sigma^2} = 20$dB.

performance for MF-ZF and ZF-ZF, as expected. On the other hand, with MF-MF and ZF-MF, binary power allocation achieves the optimal performance. For instance, with ZF-MF, it can achieve up to 25% gains in the sum rate with respect to full reflection mode. Fig. 3 shows also a performance comparison with a benchmark beamforming technique proposed in [4], where transmit precoder, receive combiner, and backscattering coefficients are jointly obtained via numerical search and iterative algorithms. Although this joint optimization provides better performance, our schemes have closed-form expressions giving analytical insights and has relatively very low complexity which is very important for backscatter communications.

Then, we show the effect of massive MIMO in enhancing the energy efficiency. Fig. 4 shows the sum rate versus $M$,

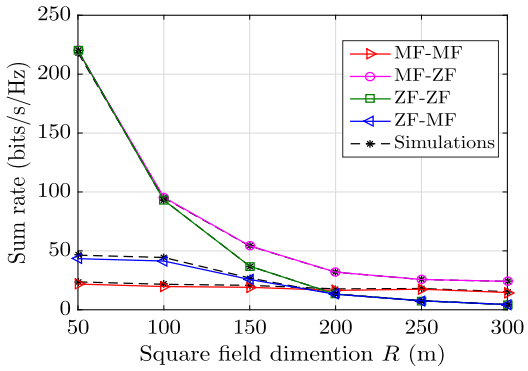


Fig. 5. Sum rate of the different schemes versus the square field dimension $R$ (m), with $M = 200$ and $K = 20$.

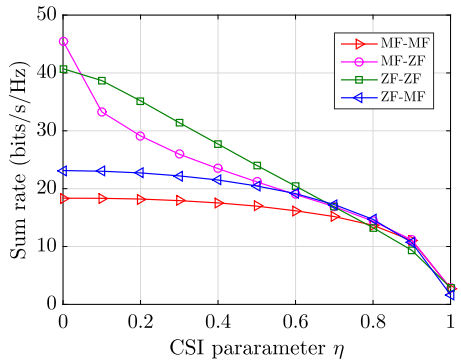


Fig. 6. Sum rate of the different schemes versus the CSI parameter $\eta$, with $M = 100$, $K = 10$, and $R = 100$m.

for $P = \frac{p}{M^2}$, where $p$ is chosen such that $\frac{p\bar{\beta}^2}{\sigma^2_{\mathcal{R}}} = 20$dB. Note that, when $M$ increases, the rates approach constant values as defined in (19) and (20), although the decrease in $P$. These results confirm the theoretical results in Section IV-A, that we can scale down the transmit power at $\mathcal{R}$ by a factor of $M^2$. Note also that ZF precoder fails to achieve satisfactory sum rate, in contrast to MF precoder, where MF-ZF achieves the best performance when considering the energy efficiency.

Fig. 5 shows the effect of increasing the service area on the performance. It is seen that the MF-ZF achieves the best performance over all range. Interestingly, although MF-MF and ZF-MF have low performance at low $R$, they achieve comparable performance when $R > 180$m. This confirms the results at low SNR as illustrated in Section IV-A.

Finally, the effect of channel estimation errors on the performance of the proposed beamforming schemes is studied. Fig. 6 shows the sum rate of the different schemes as a function of $\eta$. It is clear that MF-ZF achieves the best average improvement at $\eta = 0$. However, this performance enhancement of MF-ZF scheme diminishes with increasing $\eta$, where ZF-ZF achieves the best performance over the values up to $\eta = 0.7$. In particular, the performance gain of ZF-ZF over MF-ZF, ZF-MF, and MF-MF decreases from 21%, 55%, and 93% for $\eta = 0.2$ to 13%, 17%, and 41% for $\eta = 0.5$ to zero for $\eta = 1$. Thus, relatively accurate CSI is required to be available at $\mathcal{R}$ in order to achieve the full potential of the proposed beamforming schemes.

## VI. Concluding Remarks

This letter investigated the performance of MF and ZF beamformers in multi-tag massive MIMO monostatic backscatter networks. We derived capacity lower bounds for the different precoding and combining scenarios. The optimal backscattering coefficients that maximize the sum rate are also derived. It was concluded that whereas high spectral efficiency is desired, MF-ZF and ZF-ZF outperform MF-MF and ZF-MF schemes. However, when the energy efficiency is of more concern, MF-MF and ZF-MF achieve comparable performance. Moreover, MF-ZF was shown to achieve the best performance when both high spectral and energy efficiency is required.

## References

[1] C. Xu, L. Yang, and P. Zhang, "Practical backscatter communication systems for battery-free Internet of Things: A tutorial and survey of recent research," *IEEE Signal Process. Mag.*, vol. 35, no. 5, pp. 16–27, Sep. 2018.

[2] N. Van Huynh, D. T. Hoang, X. Lu, D. Niyato, P. Wang, and D. I. Kim, "Ambient backscatter communications: A contemporary survey," *IEEE Commun. Surveys Tuts.*, vol. 20, no. 4, pp. 2889–2922, 4th Quart., 2018.

[3] J. Kimionis, A. Bletsas, and J. N. Sahalos, "Increased range bistatic scatter radio," *IEEE Trans. Commun.*, vol. 62, no. 3, pp. 1091–1104, Mar. 2014.

[4] D. Mishra and E. G. Larsson, "Sum throughput maximization in multi-tag backscattering to multiantenna reader," *IEEE Trans. Commun.*, vol. 67, no. 8, pp. 5689–5705, Aug. 2019.

[5] D. Mishra and E. G. Larsson, "Optimal channel estimation for reciprocity-based backscattering with a full-duplex MIMO reader," *IEEE Trans. Signal Process.*, vol. 67, no. 6, pp. 1662–1677, Mar. 2019.

[6] A.-S. Bana *et al.*, "Massive MIMO for Internet of Things (IoT) connectivity," *Phys. Commun.*, vol. 37, Dec. 2019, Art. no. 100859.

[7] H. Quoc Ngo, E. G. Larsson, and T. L. Marzetta, "Energy and spectral efficiency of very large multiuser MIMO systems," *IEEE Trans. Commun.*, vol. 61, no. 4, pp. 1436–1449, Apr. 2013.

[8] I. Krikidis, "Retrodirective large antenna energy beamforming in backscatter multi-user networks," *IEEE Wireless Commun. Lett.*, vol. 7, no. 4, pp. 678–681, Aug. 2018.

[9] A. J. S. Boaventura and N. B. Carvalho, "The design of a high-performance multisine RFID reader," *IEEE Trans. Microw. Theory Techn.*, vol. 65, no. 9, pp. 3389–3400, Sep. 2017.

[10] X. Hao *et al.*, "A 43.2 $\mu$W 2.4 GHz 64-QAM pseudo-backscatter modulator based on integrated directional coupler," in *Proc. IEEE Int. Symp. Circuits Syst. (ISCAS)*, May 2018, pp. 1–5.

[11] Q. Yang, H.-M. Wang, Y. Zhang, and Z. Han, "Physical layer security in MIMO backscatter wireless systems," *IEEE Trans. Wireless Commun.*, vol. 15, no. 11, pp. 7547–7560, Nov. 2016.

[12] J. Kimionis, A. Georgiadis, A. Collado, and M. M. Tentzeris, "Enhancement of RF tag backscatter efficiency with low-power reflection amplifiers," *IEEE Trans. Microw. Theory Techn.*, vol. 62, no. 12, pp. 3562–3571, Dec. 2014.

[13] S. Lee, Y. Zeng, and R. Zhang, "Retrodirective multi-user wireless power transfer with massive MIMO," *IEEE Wireless Commun. Lett.*, vol. 7, no. 1, pp. 54–57, Feb. 2018.

[14] A. M. Tulino and S. Verdu, *Random Matrix Theory and Wireless Communications*. New York, NY, USA: Now, 2004.

[15] S. J. Thomas, E. Wheeler, J. Teizer, and M. S. Reynolds, "Quadrature amplitude modulated backscatter in passive and semipassive UHF RFID systems," *IEEE Trans. Microw. Theory Techn.*, vol. 60, no. 4, pp. 1175–1182, Apr. 2012.

[16] G. Yang, C. K. Ho, and Y. L. Guan, "Multi-antenna wireless energy transfer for backscatter communication systems," *IEEE J. Sel. Areas Commun.*, vol. 33, no. 12, pp. 2974–2987, Dec. 2015.

[17] H. Sifaou, A. Kammoun, L. Sanguinetti, M. Debbah, and M.-S. Alouini, "Max–Min SINR in large-scale single-cell MU-MIMO: Asymptotic analysis and low-complexity transceivers," *IEEE Trans. Signal Process.*, vol. 65, no. 7, pp. 1841–1854, Apr. 2017.

[18] C. Wang and R. D. Murch, "Adaptive downlink multi-user MIMO wireless systems for correlated channels with imperfect CSI," *IEEE Trans. Wireless Commun.*, vol. 5, no. 9, pp. 2435–2446, Sep. 2006.